Available online at www.sciencedirect.com

SciVerse ScienceDirect

Ceramics International 39 (2013) 5639–5650

CERAMICS INTERNATIONAL

www.elsevier.com/locate/ceramint

Electrochemical aspects and in vitro biocompatibility of polypyrrole/TiO_2 ceramic nanocomposite coatings on 316L SS for orthopedic implants

A. Madhan Kumar, N. Rajendran*

Department of Chemistry, Anna University, Chennai-600 025, India

Received 14 November 2012; received in revised form 19 December 2012; accepted 22 December 2012
Available online 10 January 2013

Abstract

With a view to developing a smart coating combining both biocompatibility and corrosion resistance over bioimplants, polypyrrole/TiO_2 nanocomposite coatings were electrochemically synthesized by cyclic voltammetric technique on 316L stainless steel (SS) in an aqueous solution of oxalic acid. The presence of TiO_2 nanoparticles in polypyrrole (PPy) matrix was confirmed using FT-IR spectroscopy and XRD analysis. The surface morphology of coated 316L SS substrates was observed by the Scanning Electron Microscopy (SEM), Atomic Force Microscopy (AFM) and Transmission Electron Microscopy (TEM). Microhardness of coated 316L SS was examined by the Vickers hardness method. The electrochemical studies were carried out using Cyclic Polarization and Electrochemical Impedance Spectroscopy (EIS) measurements. In order to describe the biocompatibility, contact angle measurements and in vitro characterization were carried out in Simulated Body Fluid (SBF) solution. The results showed that the nanocomposite coatings exhibit superior biocompatibility and enhanced corrosion protection performance over 316L SS than that of pure polypyrrole coatings.
© 2013 Elsevier Ltd and Techna Group S.r.l. All rights reserved.

Keywords: C. Corrosion; Polypyrrole; Biocompatibility; Nanoceramic TiO_2

1. Introduction

Stainless steel (SS) is one of the most adequate metallic biomaterials and is widely used in orthopedic devices, and long and short-term implants owing to its ease of fabrication, relatively low cost and reasonable corrosion resistance. Although bare 316L SS has been approved by the US Food and Drug Administration, its biocompatibility is still an issue because of the rigorous body environment [1,2]. The biocompatibility of both permanent and temporary implants has always been a concern due to the known adverse biological effects of individual metal components of stainless steel [3]. Cr (VI) is toxic and carcinogenic; nickel is accepted to be carcinogenic and provokes contact dermatitis [4,5]. Hence, it is extremely necessary to modify the surface or to develop a new kind of biomedical surface-coated materials to improve the biocompatibility of these 316L SS implants.

One way to minimize the release of corrosion products from the implant to the surrounding tissues is to apply protective coatings. Such coatings are expected to be functional with bioactive material for inducing the formation of a semi-crystalline hydroxyapatite (HA) rich layer onto the material surface, generating a natural bond to living tissues. A variety of materials have been used as coatings for 316L SS implants in order to improve its biocompatibility. Some of these consist of inorganic metal oxides such as TiO_2, ZrO_2, Nb_2O_5 [6–8]; others consisting of organic substances and also some conducting polymers such as polypyrrole (PPy) [9,10].

A PPy coating has also an excellent corrosion resistance due to its high stability, which prevent the electron exchange between the metal and the adsorbed biological species. The biocompatibility of PPy has been adequately verified [11,12]. PPy film has been used as protective coatings for Ti–Al–V

*Corresponding author. Tel.: +91 44 2235 8659; fax: +91 44 222006600.
E-mail address: nrajendran@annauniv.edu (N. Rajendran).

0272-8842/$ - see front matter © 2013 Elsevier Ltd and Techna Group S.r.l. All rights reserved.
http://dx.doi.org/10.1016/j.ceramint.2012.12.080

substrates to improve osteointegration performances [13]. Moreover, a recent study on PPy film coated implants in experimental animals showed promising results for their in vivo use [14]. However, PPy has some inherent limitations such as poor mechanical strength, processability and also the bone bonding ability which needs to be further improved. To overcome these limitations, preparation of composites with suitable insulating or conducting substrates is a widely known technique. It was reported that TiO_2 incorporation into electrodeposited PPy matrix on Pt or other metals is possible when a small amount of supporting electrolyte, whose anions distinctively adsorb on TiO_2 particles, is added [15] or by electrosynthesis under strong stirring [16]. It was also reported that the maximum amount of TiO_2 incorporated into the PPy matrix was approximately 0.44 wt% in the first case and 17 wt% in the second, which suggests that oxide incorporation is markedly influenced by the synthesis conditions. However, the incorporation of micron sized particles into the polymer matrix leads to heterogeneous distribution which in turn reduces the barrier properties. Reducing the particle dimensions into nanoscale can enhance the order of distribution and improve the barrier properties of the polymer coating.

PPy/TiO_2 nanocomposite combines the merits of PPy and nano-TiO_2 to develop the potential applications in many fields. Recently, Ferreira et al. [17] synthesized PPy/TiO_2 nanocomposite by electropolymerization on mild steel and reported that these composites can be used as an alternative material for the preparation of stainless steel surfaces for paint applications. To the best of our knowledge, the use of PPy/TiO_2 nanocomposite coatings in bioimplants is rather scarce. In addition, we have already achieved the enhanced corrosion resistance and improved bioactivity of bioimplants through various surface modification techniques under H_2O_2 treatment [18] and alkali treatment [19]. It also attempted to compare the protection efficiency and bioactivity of the newly developed implant materials with conventional implant materials under simulated physiological condition [20]. However, the aim of the present investigation is to modify the corrosion protection performance and biocompatibility of PPy film over 316L SS bioimplants by introducing TiO_2 nanoparticle and to improve the barrier effect of the polymer matrix.

2. Materials and methods

2.1. Chemicals and apparatus

Pyrrole (monomer), TiO_2 nanoparticles (anatase phase), oxalic acid and all other chemicals used in this study were purchased from Aldrich Chemical Company. The size of the TiO_2 nanoparticles used in the present investigation is about 8–10 nm. The pyrrole monomer was distilled twice while the other analytical grade chemicals were used without any further purification. All the electrosynthesis experiments were performed in an aqueous solution of 0.1 M pyrrole in 0.3 M oxalic acid prepared using ultrapure deionized water. All the experiments were carried out at room temperature and atmospheric pressure.

Electropolymerization and all other electrochemical studies were carried out in a conventional three electrode system with 316L SS substrates (composition given in Table 1) as working electrode, platinum wire as counter electrode and saturated calomel electrode (SCE) as reference electrode, of which all potentials were referenced. The working electrode constructed from 316L SS substrate with an exposed area of 1 cm^2 was embedded in Teflon holder. Prior to each electrochemical experiment, this working electrode was mechanically polished with abrasive paper using grit size from 600 to 1200 grade and cleaned in 1:1 acetone/ethanol mixture in an ultrasonic bath to remove impurities, rinsed with water and then dried in air. The Simulated Body Fluid (SBF) solution was used as electrolyte for electrochemical and in vitro characterization.

The potentiostat (model PGSTAT 12, Autolab, The Netherlands B.V.) was used for electropolymerization and other electrochemical studies. This system was interfaced with a personal computer to control the experiments and the data were analyzed using dedicated software (GPES version 4.9.005). The analysis of the impedance spectra and fitting of the experimental results to equivalent circuits were performed using ZSimpWin 3.21, which allowed the chi-square (χ^2) value to judge the quality of the equivalent circuit fitting.

2.2. Preparation of PPy/TiO_2 nanocomposite coatings

The PPy/TiO_2 nanocomposite coatings were synthesized by electropolymerization on 316L SS substrate from an aqueous oxalic acid solution (0.3 M) containing polypyrrole (0.1 M) with different amounts of TiO_2 nanoparticles (1, 5, 10, 15 and 20 mg) using cyclic voltammetry in the potential regions (-0.6 V to $+0.7$ V, versus SCE) at a scan rate of 50 mV s^{-1} over 10 cycles with constant stirring. After electrodeposition of the films, polymer coated electrodes were removed from the polymerization medium and rinsed with deionized water to remove monomer molecules before being dried in air. For comparison, pure PPy coating was also electropolymerized in the same condition

Table 1
Composition of 316L SS substrate.

Alloy	Main alloying elements (wt%)						
	Cr	Ni	Mo	N	C	Mn	Fe
316L SS	17.20	12.60	2.40	0.02	0.03	1.95	balance

as mentioned above, but without TiO_2 nanoparticles in polymerization electrolyte solution.

The thickness of the PPy/TiO_2 and also of the PPy coatings was measured by an Elcometer instrument. The standard deviation of thickness values is about ± 0.5 μm. The average thickness of PPy and PPy/TiO_2 nanocomposite coatings was approximately 8.17 μm and 8.40 μm, respectively.

2.3. Characterization of PPy and PPy/TiO_2 nanocomposite coatings

In order to characterize the PPy/TiO_2 nanocomposite coatings, the highest addition (20 mg) of TiO_2 nanoparticles in the PPy has been used for FTIR, XRD, FE-SEM/EDAX, TEM analyses and electrochemical measurements.

The structures of PPy and PPy/TiO_2 nanocomposite coated 316L SS substrates were analyzed by FTIR reflectance spectrophotometry (PerkinElmer, Spectrum One, with universal ATR attachment with a diamond and ZnSe crystal). The surface topography was analyzed through AFM using the SII (Seiko instruments, Japan) instrument. The images were acquired by non-contact mode using Au coated silicon cantilevers with a spring constant of 1.6 N/m at a resonance frequency of 26 kHz under air atmosphere at room temperature. The deviation of roughness values in AFM investigation is ± 5 nm. The crystallographic patterns of coated 316L SS substrates were analyzed by XRD (RINT2500, Rigaku Co., Tokyo, Japan; CuKα, 40 kV, 20 mA).

The surface morphologies of polymer coated 316L SS were investigated by Field-Emission Scanning Electron Microscope (FE-SEM) from Hitachi, which was generally operated at 10 keV accelerating voltage and secondary electron imaging mode. The distribution of TiO_2 nanoparticles on the PPy matrix was observed by Transmission Electron Microscopy (TEM) from TEM-2100F, which was operated with bright field image mode at 20 keV accelerating voltage.

Contact angles were measured by a sessile drop method with a Kruss G10 contact angle apparatus. A drop of SBF (5 μl) was placed on the coated substrates and was photographed immediately after positioning. The images of drops were processed by the image analysis system, which calculated contact angles from the shapes of the drops with an accuracy of $\pm 0.1^{\circ}$. Uncoated steel substrate was considered as control. To achieve an accurate value, ten measurements were collected for each substrate.

Microhardness test was also carried out with a Vickers pyramid indenter, by The Ever one, Model no. MH-3 (Germany) ultramicrohardness tester in order to evaluate the hardness of the coated substrates. Hardness measurements were performed on the surfaces at a load of 0.5 kgf and dwell time of 12 s. The Vickers hardness (HV) value was calculated by dividing the indentation force by the surface of the imprint observed at the microscope. For each substrate, at least 10 measurements were made at various sites.

2.4. Electrochemical measurements

Electrochemical studies of uncoated and coated 316L SS substrates were carried out in SBF solution by cyclic polarization techniques and electrochemical impedance spectroscopy (EIS) measurements. The anodic and cathodic polarization curves were recorded by changing the electrode potential from open circuit potential (OCP) with a constant sweep rate of 0.167 mV s^{-1}. Electrochemical impedance measurements were recorded at OCP at various exposure times and in the frequency range from 10^4 to 1 mHz using AC amplitude of 10 mV. In order to test the reproducibility of the results, the experiments were performed in triplicate.

2.5. In vitro characterization

The preparation of SBF and the procedure for conducting the in vitro test was adopted using an earlier report [21]. The PPy and PPy/TiO_2 nanocomposite coated substrates were immersed in SBF for a period of 7 days to evaluate their ability to favor apatite deposition. SBF was renewed on alternate days to avoid precipitation. The temperature of the immersed samples was maintained at 37 °C, similar to human body temperature throughout the experimental time.

3. Results and discussion

3.1. Electropolymerisation of PPy and PPy/TiO_2 nanocomposite coatings

Prior to electropolymerization of *PPy and PPy/TiO_2* nanocomposite coatings, the 316L SS working electrode was partially passivated in 0.3 M oxalic acid solution by cycling the potential between -0.6 and $+0.7$ V at a low scan rate of 20 mV s^{-1}. In the case of 316L SS, anodic or chemical oxidation is accompanied by dissolution of the metal. In general, the oxidation potential of most monomers is in the region of metal dissolution. The released metal ions could affect the oxidation of the monomer and thus the growth of an adherent polymer film. Passivation of stainless steel electrode in oxalic acid medium before electropolymerization is also reported and voltammograms recorded in monomer free oxalic acid solution during passivation procedure are the same as those obtained by other researchers [22]. Fig. 1 shows the cyclic voltammograms (CVs) which were recorded during continuous voltammograms in a solution of pyrrole (0.1 M) in aqueous oxalic acid (0.3 M) in the absence and presence of different amount of TiO_2 nanoparticles on 316L SS substrates respectively. As can be seen the monomer oxidation process took place as the potential increases around 0.6 V. Here, it is important to mention that the addition of TiO_2 nanoparticles into electrolyte solution affected the electropolymerization process. Moreover, the

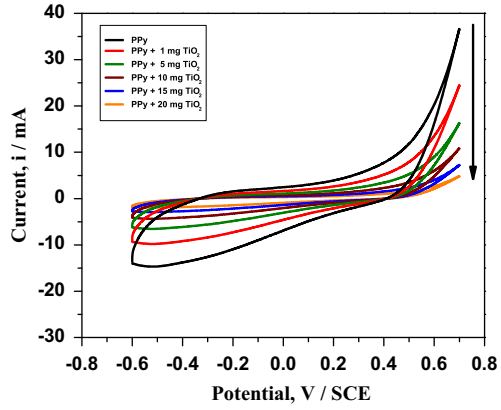

Fig.1. The growth of pure PPy and PPy/TiO_2 nanocomposite film during continuous voltammograms in a solution of 0.1 M of pyrrole in 0.3 M of oxalic acid without and with different amount of TiO_2 in the electrolyte solution at 50 mV/s.

consumed charge in electropolymerization of pyrrole in the presence and absence of TiO_2 nanoparticles was different which can be explored by the influence of TiO_2 nanoparticles. Besides, the current density decreased with increasing concentration of TiO_2 nanoparticles in electrolyte solution. This result indicated that the addition of TiO_2 nanoparticles significantly decrease the current density of the monomer oxidation process at the same applied potentials and decreases the conductivity of electrolyte to some extent. Moreover, TiO_2 nanoparticle might act as a barrier and reduce direct interaction between monomers and the surface of steel as working electrode [23]. Visually, the surface was uniform, smooth, and glossy. In order to examine the adhesion of these PPy coatings over 316L SS substrates, the ASTM D 3359 standard tape adhesion test was applied, and all the coatings exhibited no failed regions, 5B, which implies good adhesive strength of PPy coating towards 316L SS surface.

The thickness of the PPy and PPy/TiO_2 nanocomposite coatings at the 316L SS surface can be calculated from the charge consumed (Q) during the electrodeposition of polymer film (the overall charge that passed during the anodic sweeps of potential) using Faraday's law. According to the following equation,

$$d_n = Q_a M / nF\rho \quad (1)$$

Considering a value of 2 for n and 108 for molecular weight of pyrrole, the polymer film thickness can easily be calculated using the value of about 1.30 g/cm^3 for density of PPy at 25 °C. The average thickness of PPy and PPy/TiO_2 nanocomposite coatings was found to be about 8.25 μm and 8.48 μm, respectively. This result is consistent with the results obtained from thickness measurements using Elcometer instrument.

3.2. FT-IR analysis

Fig. 2a shows the FTIR spectra of pure PPy and PPy/TiO_2 nanocomposite coated 316L SS substrates,

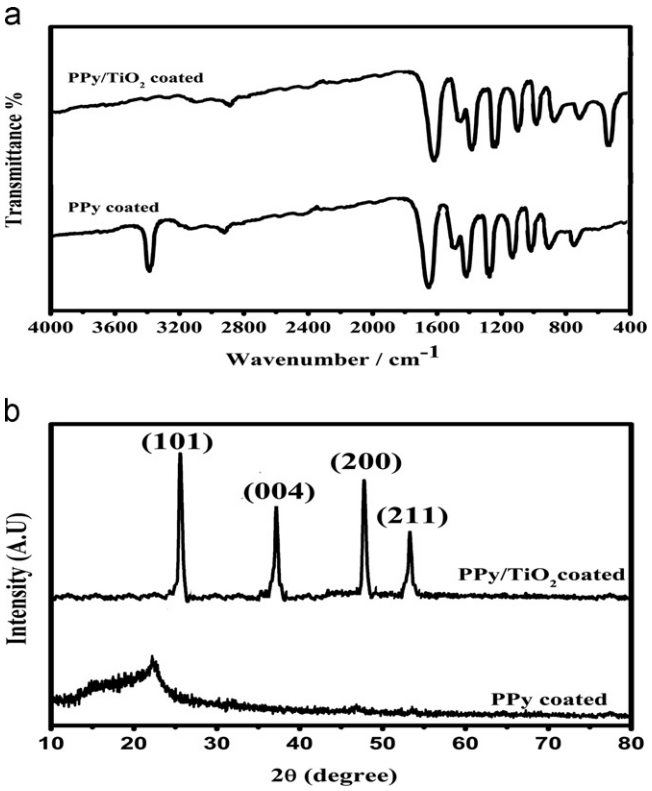

Fig. 2. FT-IR spectra and XRD patterns of Pure PPy and PPy/TiO_2 nanocomposite coated.136L SS.

respectively. In the spectra of pure PPy, the characteristic peaks at 3400 and 1640 cm^{-1} were assigned to N–H stretching and C–N in plane bending vibration and the peaks at 1548 and 1430 cm^{-1} were attributed to C=C and C–N stretching vibration in pyrrole ring, respectively. The peaks at 1324 and 1023 cm^{-1} were corresponded to C–N bending and C–O–C stretching vibration respectively. The C–H in-plane bending vibration and C–H out-of-plane bending vibration were observed at 1175 and 910 cm^{-1}, respectively. The IR absorption band at 790 cm^{-1} was represented by the five-membered heterocyclic ring with α substitution which indicated that the PPy chain has α position conjugation chain structure [24].

In the case of PPy/TiO_2 nanocomposites, the N–H stretching vibration peaks observed at 3400 cm^{-1} had disappeared and all the characteristic peaks of PPy were found to be shifted to a lower wave number compared with pure PPy. In addition, the characteristic peak of the TiO_2 nanoparticles was observed at 570 cm^{-1}, indicating the presence of TiO_2 in polymer matrix. These results indicated that a strong interaction exists at the interface of PPy and nano-TiO_2 [25].

3.3. X-ray diffraction analysis

Fig. 2b displays X-ray diffraction pattern of pure PPy coated 316L SS, which has a broad peak at about $2\theta = 24.5°$, a characteristic peak of amorphous polypyrrole

[26]. The typical X-ray diffraction pattern of PPy/TiO_2 nanocomposite coated 316L SS clearly revealed that the PPy deposited on the surface of TiO_2 nanoparticles has no effect on the crystallization behavior of TiO_2 nanoparticles. Moreover, the observed strong diffraction peaks at 2θ values 25.3, 37.8, 48 and 55.1 corresponding to the planes of (1 0 1), (0 0 4), (2 0 0) and (2 1 1) indicated that the TiO_2 present as anatase phase in the nanocomposite coatings. The average crystallite size of TiO_2 nanoparticles has been calculated using Scherer's equation [27].

$$D_{hkl} = k\lambda/[B\cos\theta] \quad (2)$$

where B is the full width half-maximum (FWHM) of the peaks of the pure diffraction profile in radians, k is a constant (shape factor 0.89), λ is the wavelength of the X-rays, θ is the diffraction angle and D_{hkl} is the average diameter of the crystallite. From the estimated data, the crystallite size of TiO_2 in the nanocomposite was about 9.2 nm.

3.4. SEM and TEM analysis

Fig. 3(a and b) shows the SEM micrographs of the PPy and PPy/TiO_2 nanocomposite coated 316L SS. In the case of the pure PPy coated 316L SS, the cauliflower like morphology constituted by micro-spherical grains with variable particles size from 10 to 20 μm was observed. The film was rough and irregular in nature. It has been reported that this cauliflower morphology is associated with the dopant intercalation difficulty in the disordered polymeric matrix [28]. However, the morphology of PPy/TiO_2 nanocomposite coated 316L SS was slightly varied from that of the pure PPy coated 316L SS. The morphology patterns of the micro-spherical grains were seen as smooth and compact, and size varied from 2 to 10 μm. The difference in the particle size was due to the presence of TiO_2 nanoparticle in PPy matrix. The chemical composition of PPy/TiO_2 nanocomposite was examined by EDAX analysis. The result indicates the existence of elements Ti from TiO_2, C, O, and N from pyrrole.

Fig. 4 shows TEM micrographs of the PPy/TiO_2 nanocomposite coated 316L SS. In TEM image of PPy/TiO_2 nanocomposite, the lighter portion showed polymer whereas, the dark portion indicated nanoparticles. It can be seen that the TiO_2 nanoparticle with grain size around 10 nm was uniformly dispersed in PPy matrix. The distribution pattern between TiO_2 nanoparticles and the conducting polymer showed that all TiO_2 nanoparticles were encapsulated by PPy. There were no separate TiO_2 nanoparticles observed, which ensure the uniform distribution of nanoparticles into polymer matrix [29].

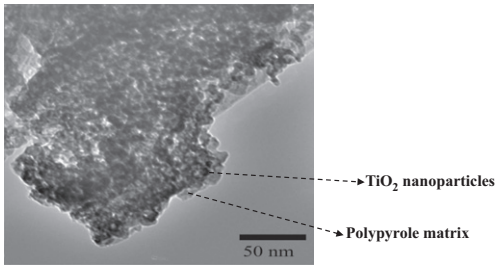

Fig. 4. TEM images of PPy/TiO_2 nanocomposite coated 316L SS.

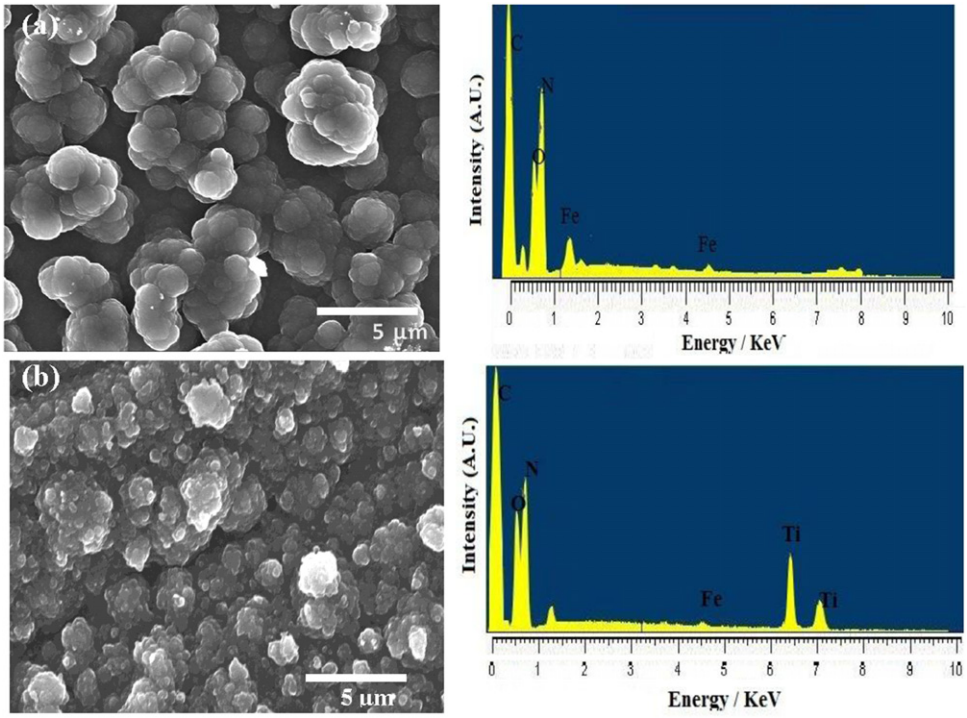

Fig. 3. FE-SEM images with EDAX results of Pure PPy and PPy/TiO_2 nanocomposite coated 316L SS.

3.5. AFM analysis

Fig. 5a shows AFM topographic images of the uncoated 316L SS substrates which revealed that the flat substrate consists of small nodule-like topography that appear to be ordered along the polishing lines. AFM images of PPy coated 316 SS (Fig. 5b) showed the non-uniform and island like topographic surface. The average diameter of the individual grains was ca 70–100 nm. In the case of PPy/TiO_2 nanocomposite coated 316L SS (Fig. 5c), uniform and a large number of individual small grains were observed with average diameter of individual grains of about 50–60 nm. This result revealed that the presence of TiO_2 nanoparticles considerably influences the PPy topography.

3.6. Hardness test

Hardness is the important parameter to bioimplants for giving the information about the load bearing tendency when it is implanted into human body under stress. Fig. 6 illustrates the Vicker microhardness for uncoated and coated 316L SS substrates. The Vicker hardness value of uncoated 316L SS was found to be 1860 MPa and it is in good agreement with the previous reports [30,31]. The PPy and PPy/TiO_2 coated 316L SS substrates exhibit higher hardness value which were found to be 2550 MPa and 3850 MPa, respectively. In addition, the hardness value increases with increasing TiO_2 nanoparticles in PPy coatings. It is already well known that the hardness value of the coating used in corrosion protection applications should be in the range of 250–750 HV (2452–7355 MPa). However in the case of orthopedic applications, increasing hardness value leads to lowering the ductility which in turn causes

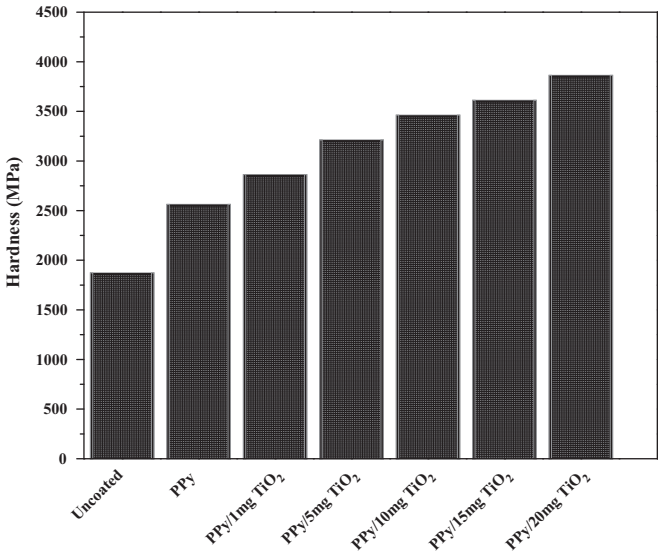

Fig. 6. Microhardness values for uncoated, pure PPy and PPy/TiO_2 nanocomposite coated 316L SS.

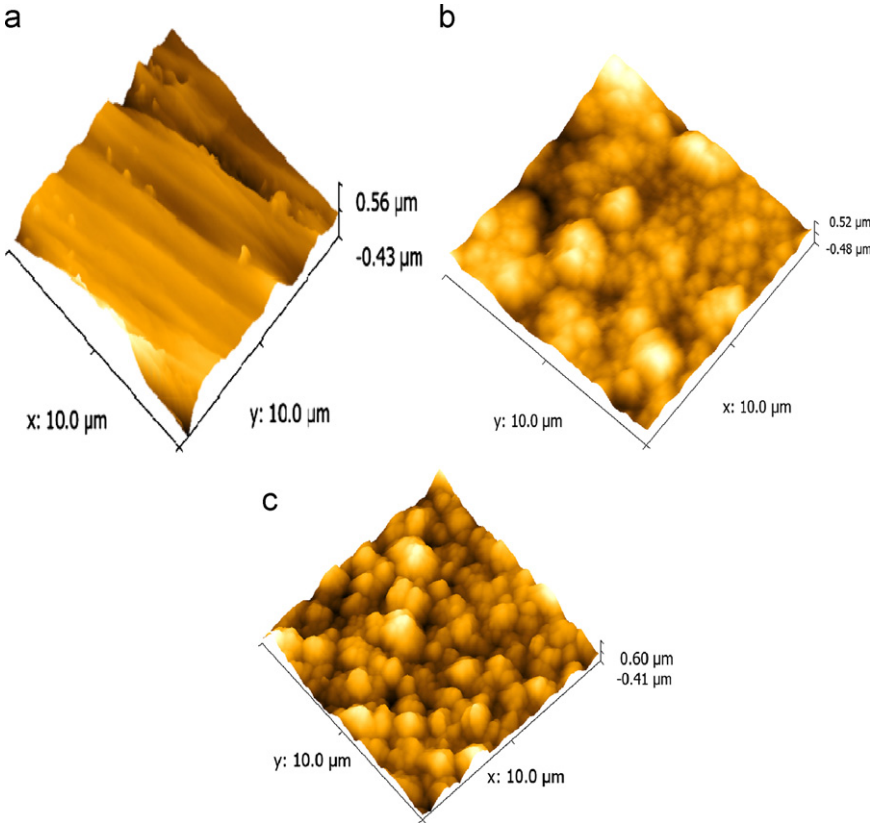

Fig. 5. AFM topographic images of (a) uncoated, (b) Pure PPy coated and (c) PPy/TiO_2 nanocomposite coated 316L SS.

stress shielding effect which is harmful and reduce the life expectancy of bioimplants. Hence, the coatings exhibiting the hardness values of about 2500–4000 MPa are more favoured for orthopedic applications. It has been already reported that the more compact and smaller grain size of the PPy coating possesses higher hardness value [32]. Compared to pure PPy coatings, nanocomposite coatings exhibit smaller grain size and more compact morphology, which was confirmed by SEM and AFM studies. This result indicated that the addition of TiO_2 nanoparticles increases the microhardness by approximately 56% due to densification of polymer matrix [33].

3.7. Electrochemical characterization

Fig. 7 shows cyclic polarization curves of the pure PPy, PPy/TiO_2 coated and uncoated 316L SS substrate immersed in SBF solution. The polarization curve of coated 316L SS substrate was appreciably different from that of the uncoated 316L SS substrate, indicating that PPy coatings have an effect on corrosion behavior. In addition, a distinct passivation region was present for the coated 316L SS substrates, whereas, no definitive passivation region was found for the uncoated 316L SS substrates, which indicate that the PPy coatings influenced the corrosion behavior. It is well known that the PPy chain stores more charge and thus makes the potential of the 316L SS poise in a more positive value. It is believed that the compounds with conjugated bonds adsorb better on metal surface due to higher number of electrons. In addition, charge conduction in the pyrrole facilitates charge delocalization which hinders formation of localized anodic or cathodic regions. It was observed that the corrosion potential presented a displacement to the nobler direction when the surface was covered by PPy up to 150 mV, and this displacement was high in the case of PPy/TiO_2 nanocomposite coated 316L SS substrates. These shifts in the corrosion potential indicated the excellent corrosion protection performance of the metal surface when the composite was deposited. It can also be clearly seen that the values of the I_{corr} of PPy and PPy/TiO_2 nanocomposite coated 316L SS were lower than that of the uncoated 316L SS substrate. Especially for the PPy/TiO_2 nanocomposite coated 316L SS, the I_{corr} was almost lower by an order of magnitude compared to the uncoated 316L SS substrate. Since the I_{corr} values are directly proportional to the corrosion rate, the nanocomposite coating provided enhanced corrosion resistance to 316L SS than PPy coatings.

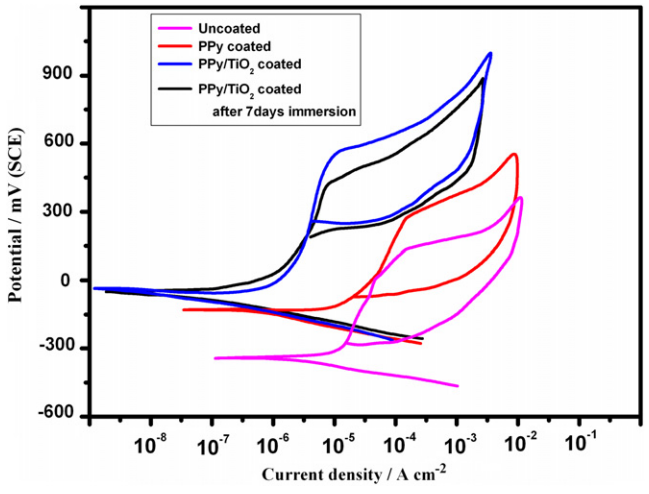

Fig. 7. Cyclic polarization curves for uncoated, pure PPy and PPy/TiO_2 nanocomposite coated 316L SS.

Moreover, the breakdown potential of the coated 316L SS related to oxygen evolution in the metal coating interface, from the electrolyte may be accessed through pores or diffusion through the film, which leads to the blistering of the coating [34]. An analysis of the breakdown potential (E_b) values revealed that the uncoated 316L SS substrate exhibit a very low value compared to the PPy coated 316L SS, providing a superior breakdown potential of 300 mV and the PPy/TiO_2 nanocomposite coated 316L SS reaches the highest value of 600 mV providing a wide passivity range. Further, the repassivation potential for the uncoated and PPy coated 316L SS were – 304 and – 70 mV respectively. In the case of PPy/TiO_2 coated 316L SS substrate, the repassivation potential was shifted to nobler direction, which suggested the improved passivation behavior of coated 316L SS substrates. In general, the area under the hysteresis loop between the breakdown potential and the repassivation potential is a direct measure of the corrosion resistance of the material [35]. A large hysteresis loop was observed for uncoated 316L SS, whereas in the case of PPy coated 316L SS the loop obtained was small. This indicates that the uncoated 316L SS is more susceptible to corrosion in SBF solution compared with the PPy coated 316L SS. It is interesting to note that breakdown and repassivation potential of PPy/TiO_2 coated 316L SS after 7 days of immersion was almost same as immediate immersion, which clearly revealed that the passivation behavior of PPy/TiO_2 coated 316L SS does not undergo any change with increasing exposure time.

Fig. 8 shows the Bode representation of uncoated and coated 316L SS after immediate immersion in SBF solution. The Bode phase angle of uncoated substrate started around 0° in the higher frequency region, it reached −80° in middle frequency region and it was constant up to lower frequency region. It showed that the passive layer was covered on the uncoated substrate, and this passive layer was homogeneous in nature. The PPy and PPy/TiO_2 nanocomposite coated substrate exhibited considerable shift in the phase angle compared to uncoated substrate. The phase shift may be attributed to a physical change in the polymer coating due to the interaction of the ions present in the electrolyte. At high frequency region, the phase angle was close to 10°, and it gradually decreased to the value of −20° and remained stable for a short range of frequency, thus making a plateau, whereas at low

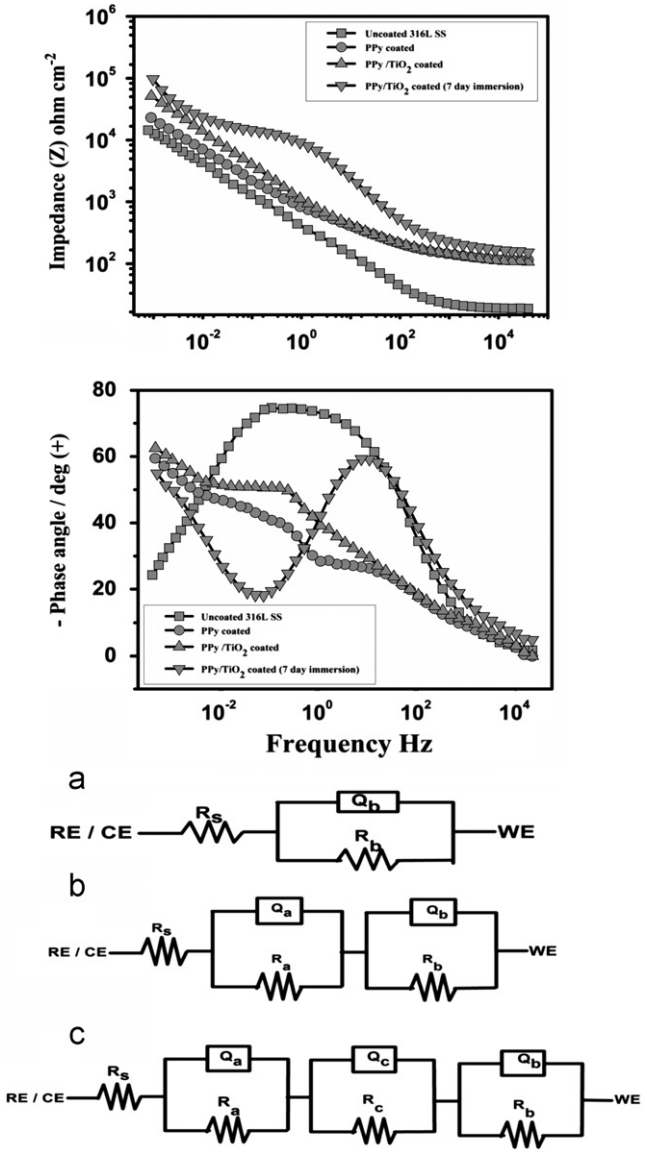

Fig. 8. Impedance spectrum of uncoated, PPy coated and PPy/TiO_2 nanocomposite coated 316L SS surface immersed for 7 days in SBF solution, (a) equivalent circuit for uncoated, (b) equivalent circuit for coated 316L SS and (c) equivalent circuit for coated 316L SS after immersion in SBF.

frequency region, the phase angle gradually decreased and attained a minimum value of -60°. This behavior indeed confirmed the presence of PPy and PPy/TiO_2 coated layer on the substrate. In the Bode resistance plot of uncoated and coated substrate at immediate immersion in SBF solution, PPy and PPy/TiO_2 coated 316L SS exhibited higher resistance compared to uncoated substrate. The EIS spectra were analyzed with an equivalent circuit, and the curve fitting was performed for all the substrates which showed an excellent agreement between the experiments and the fitting. The fitted values are given in Table 2. The PPy/TiO_2 coated 316L SS shows higher charge transfer resistance values compared with uncoated and PPy coated substrate. This revealed that the nanocomposite coated 316L SS substrate exhibited better corrosion resistance than PPy coated and uncoated 316L SS substrates. Fig. 8(b and c) displays the fitted equivalent circuits which are corresponding to R_s (R_bQ_b) for uncoated substrate and R_s (R_cQ_c) (R_bQ_b) for coated substrate, where R_s, R_b, R_c represent the solution resistance, charge transfer resistances of barrier and coated layers, and Q_b and Q_c are the double layer capacitance of barrier and coated layers respectively.

3.8. In vitro characterization

To examine the biocompatibility of PPy/TiO_2 nanocomposite coatings over 316L SS substrates, contact angle measurements and in vitro studies were performed in simulated body fluid (SBF) solution for 7 days. The bioactivity of the coatings was supported by the formation of an apatite like layer on the surface of the sample after immersion in SBF solution. It has been demonstrated that bone-like hydroxyapatite exhibits good osteoconductivity and has a high affinity to living bone cells [36,37]. It is effective in attracting cells and allows osteoblasts to form a new bone tissue. Thus, the formation of the bone-like hydroxyapatite layer on the surface of implant is an essential requirement for osseointegration between the implant and the living bone tissue. The FT-IR spectra of PPy/TiO_2 coated 316L SS substrates on immersion in SBF after 7 days are shown in Fig. 9a. The broad absorption band around 3500–3600 cm^{-1} corresponds to OH^- stretching. The peak at 579 cm^{-1} results from the υ4 mode of O–P–O bending, whereas the peak observed at 1008 cm^{-1} indicated the υ3 band of P–O stretching mode [38]. The peaks approximately at 1450 cm^{-1} and 850 cm^{-1} correspond to the υ3 vibration mode of carbonate incorporated in the apatite [39]. Hence, the appearance of the phosphate and carbonate absorption bands in the spectra of the coated 316L SS substrates after soaking in SBF solution confirmed the formation of calcium and phosphate layer.

In order to confirm the crystalline nature of hydroxyapatite growth over PPy/TiO_2 coated 316L SS substrates, X-ray diffraction analysis were performed after 7 days of immersion in SBF solution, and the result is shown in Fig. 9b. The diffractogram of coated 316L SS substrates exhibits the characteristic peaks of HA at 24.20°, 31.52°, 34°, 35.93°, 41.10°, 54.18°, 65.86° and 71.94°, which correspond to semi-crystalline HA [40]. Moreover, the diffraction peaks corresponding to anatase phase of titanium dioxide were also observed with HA, which revealed that the semicrystalline HA with titanium dioxides is present on the coated surface after immersion in SBF solution.

Surface hydrophilicity of implant material is a key factor to influence the biocompatibility [41]. The effect of TiO_2 nanoparticles on surface wettablity of PPy coating was evaluated by contact angle measurements and the acquired data are shown in Table 3.The contact angle of uncoated 316L SS was found to be 82.3°, which indicated the hydrophobic nature of 316L SS [42], whereas the PPy coated substrate exhibited lower contact angle which was

Table 2
Electrochemical impedance parameter of uncoated and coated 316 L SS immediate immersion and after 7days of immersion in SBF solution.

316L SS	R_s (Ω cm^2)	Q_a (μF cm^{-2})	n_a	R_a (kΩ cm^2)	Q_c (μF cm^{-2})	n_c	R_c (kΩ cm^2)	Q_b (μF cm^{-2})	n_b	R_b (kΩ cm^2)
Uncoated	83	0.08	0.87	14.6	—	—	—	—	—	—
PPy coated	102	0.87	0.89	23	0.93	0.74	48	—	—	—
PPy/TiO_2 coated	104	0.56	0.93	51.2	0.85	0.81	68	—	—	—
PPy/TiO_2 coated (after 7 days immersion in SBF)	106	0.32	0.84	97.3	0.47	0.68	118.6	36.8	0.54	21

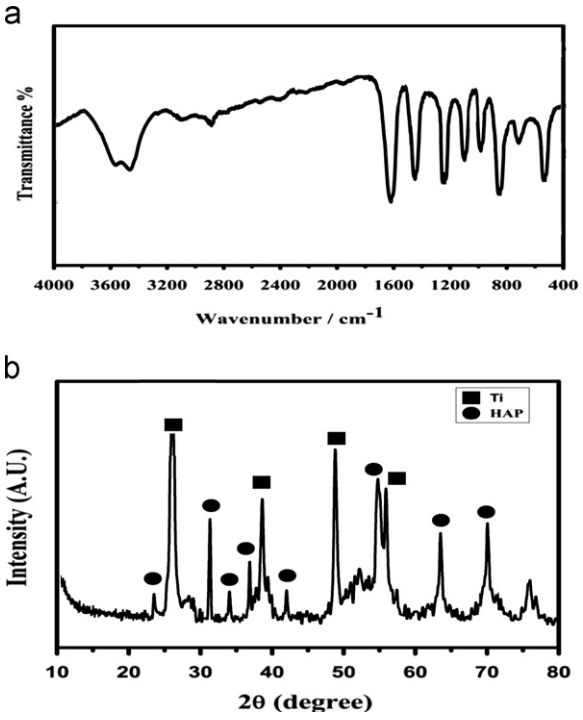

Fig. 9. FT-IR spectra and XRD patterns of PPy/TiO2 nanocomposite coated 316L SS after 7days immersion in SBF solution.

Table 3
Contact angle values of uncoated and coated 316L SS substrates.

S. No	Sample	Contact angles
1	Uncoated 316L SS	82.3
2	Pure PPy	37.4
3	PPy+1 mg TiO_2	19.3
4	PPy+5 mg TiO_2	17.6
5	PPy+10 mg TiO_2	15.8
6	PPy+15 mg TiO_2	14
7	PPy+20 mg TiO_2	13.2

found to be 32.7° due to the presence of amine group in the polymer matrix. It is well known that functional groups like amine, carboxyl, and hydroxyl groups have a hydrophilic character. However, the PPy/TiO_2 nanocomposite coatings exhibited lower contact angle than PPy coated substrate. This behavior is due to the hydrophilic nature of anatase TiO_2 in PPy matrix [43]. It has already been reported that the hydrophilic nature of coatings over implants improves ion exchange behavior from SBF solution, which in turn enhances the apatite growth [44]. In addition, it was clearly observed that the contact angle values decreased with increasing TiO_2 nanoparticles into PPy coatings. The improved hydrophilicity of PPy coating after adding proper amount of TiO_2 nanoparticles agrees well with the result of microhardness test as mentioned in the previous section. These results indicated that the incorporation of TiO_2 in polymer matrix enhances the hydrophilic nature, which further corroborates the enhanced bioactivity of nanocomposite coatings.

Fig. 10(a and b) shows the SEM image obtained for the PPy and PPy/TiO_2 coated 316L SS substrates immersed in SBF for 7 days, which revealed that the surface of the film was covered by a new layer of material that appeared to be constituted by globular shaped crystallites. This new layer corresponded to an apatite like structure and it was constituted by small crystallites [45]. The cross section SEM image of coated 316L SS after 7 days of immersion in SBF solution is shown in Fig. 10(c and d). In the case of PPy coated 316L SS substrates, the agglomeration of spherical particles was exhibited due to rough morphology of PPy surface, whereas in the case of nanocomposite coated substrates, uniform spherical particles were clearly observed due to smooth surface of the film surface which was confirmed by SEM and AFM results. In addition, the anatase TiO_2 nanoparticles present in the PPy matrix was necessary to induce easy deposition of apatite on the surface in SBF [46]. The in vitro test clearly revealed that the polymer coatings induced the formation of semi-crystalline hydroxyapatite rich layer on the substrate surface as a result of the chemical reaction of the particles with the surrounding body fluid. The apatite particles with sizes of about 1 μm were dispersed on the surface. The EDAX observation corroborates the presence of Ca and P elements on the surface of coated substrates which are subjected to immersion in SBF solution for 7 days. The PPy/TiO_2 nanocomposite coated surface shows higher Ca and P element peak intensity compared with PPy coated substrate. The corresponding EDAX spectrum shows Ca and P, together with a significant decrease of Ti percentage. The increasing concentration of Ca and P indicated the formation of an apatite like material on the surface. In addition, it was clearly shown that that n (Ca)/n (P) atom ratio is about 1.67, which is very similar to that of hydroxyapatite (HA).

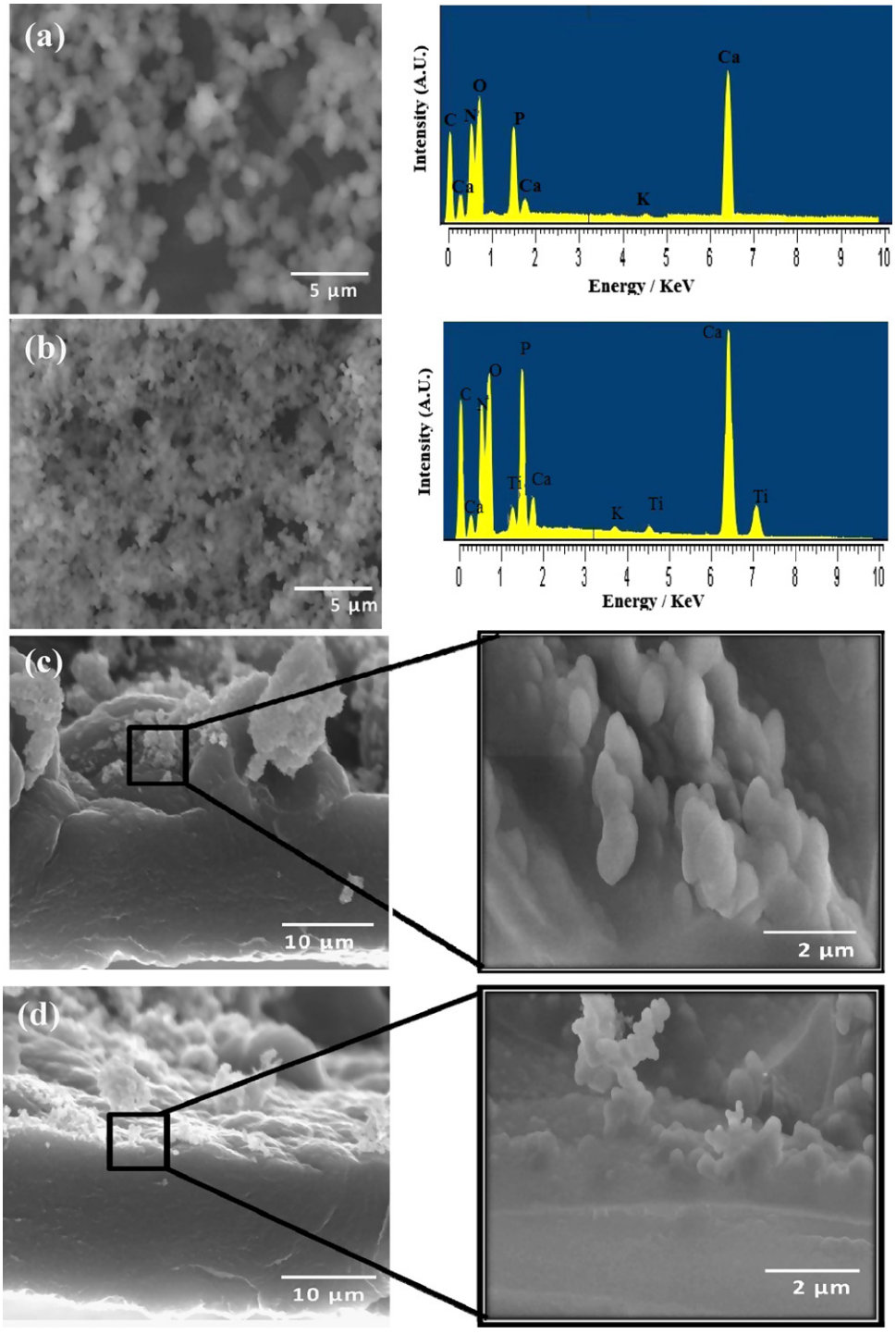

Fig. 10. FE-SEM images of (a), (c) Pure PPy and (b), (d) PPy/TiO_2 nanocomposite coated 316L SS after 7 days of immersion in SBF solution.

The PPy/TiO_2 coated 316L SS immersed in SBF solution for 7 days showed the maximum phase angle value of -35° in the high frequency region and, the phase angle value of -55° in the middle frequency region, whereas in the low frequency region, a new time constant with distinct phase angle behavior was observed. This pattern was similar to that has been ascribed earlier due to the presence of coating layer followed by an initiation of a new apatite like layer [21]. The growth of a new layer over PPy/TiO_2 coating can be associated with the apatite growth. The formation of apatite layer was the characteristic of a phase angle shift at low frequencies. This shift in the phase angle can be attributed to a growth of apatite over the PPy layer [47]. The increase in the capacitance values of the apatite layer was indicative of a growth in the layer. The impedance spectra of coated substrate immersed in SBF solution for 7 days values were fitted by the equivalent circuit model and the values are summarized in Table 2. The fitted equivalent circuit model for

all the substrate was R_s (R_aQ_a) (R_bQ_b) and R_s (R_aQ_a) (R_cQ_c) (R_bQ_b) corresponding to uncoated and PPy coated 316L SS. When compared to immediate immersion, the substrates immersed in 7 days exhibited two more elements viz., R_a and Q_a, which represent the charge transfer resistance and the double layer capacitance of apatite layer over the PPy/TiO_2 coated surface. It is observed from the table that the increase in the C_{dl} value for PPy/TiO_2 coated 316L SS reveals higher apatite forming ability compared to uncoated substrate. This impedance results were in good agreement with obtained SEM results. The lower resistance values for the uncoated 316L SS indicate that the susceptibility towards the corresponding ions present in the electrolyte can attack the surface and this is attributed to the thinning of the passive film. It is to be noted here that the resistance of the PPy/TiO_2 coated substrate has a higher value and it is consistent with the insulating nature of the coatings. The surface indicated that the barrier effect on the films remains unaltered, which impedes the ingress of anions in the electrolyte from attacking metal-coating interface. PPy/TiO_2 coated substrate after immersion of 7 days showed a three-time constant, which can be attributed to the formation of apatite layer from the interaction of solution ion with the titanium dioxide from polymer coating [48]. The interaction of solutions was generally identified by a phase shift at higher frequency region which can be attributed to a physical change in the porous coating due to the interaction of the solution ions present in the solution [49].

4. Conclusions

The electrodeposition of PPy/TiO_2 nanocomposite coatings on 316L SS substrates was prepared by cyclic voltammetric technique. The presence of TiO_2 nanoparticle in PPy matrix was confirmed by FT-IR, SEM and AFM analysis. From the TEM and XRD results, the size of the TiO_2 nanoparticle was observed about 10 nm. Microhardness of nanocomposite coating was examined using Vickers hardness method, which revealed the beneficial role of TiO_2 in the PPy matrix. The electrochemical studies revealed that the presence of TiO_2 nanoparticle in PPy matrix enhanced the corrosion protection performance of the coated 316 L SS substrates. The in vitro characterization and contact angle measurements revealed that the formation of homogeneous and higher growth of HA over the nanocomposite coated 316L SS in SBF is due to the hydrophilic, more compact and smooth morphology of the PPy/TiO_2 coated surface. Based on the above findings, the PPy/TiO_2 nanocomposite coating has better biocompatibility and enhanced corrosion resistance which is considered as the potential candidate as a coating material for 316L SS bioimplants.

Acknowledgment

The authors would like to thank the facilities provided at Department of Chemistry, Anna University by DST-FIST and UGC-DRS.

Reference

[1] G. Mani, M.D. Feldman, D. Patel, C.M. Agrawal, Coronary stents: a materials perspective, Bio Materials 28 (2007) 1689–1710.
[2] T. Hryniewicz, R. Rokicki, K. Rokosz, Surface characterization of AISI 316L biomaterials obtained by electropolishing in a magnetic field, Surface and Coatings Technology 202 (2008) 1668–1673.
[3] B. Liu, Y.F. Zheng, Effects of alloying elements (Mn, Co, Al, W, Sn, B, C and S) on biodegradability and in vitro biocompatibility of pure iron, Acta Biomaterialia 7 (2011) 1407–1420.
[4] B. Karim, J. Jean, D. Mainard, P. Elisabeth, N. Patrick, Evaluation of the effect of three surface treatments on the biocompatibility of 316L stainless steel using human differentiated cells, Bio Materials 17 (1996) 491–500.
[5] T. Tucken, Polypyrrole films on stainless steel, Surface and Coatings Technology 200 (2006) 4713–4719.
[6] S. Nagarajan, N. Rajendran, Surface characterisation and electrochemical behavior of porous titanium dioxide coated 316L stainless steel for orthopedic applications, Applied Surface Science 255 (2009) 3927–3932.
[7] S. Nagarajan, N. Rajendran, Sol–gel derived porous zirconium dioxide coated on 316L SS for orthopedic applications, Journal of Sol–Gel Science and Technology 52 (2009) 188–196.
[8] S. Nagarajan, V. Raman, N. Rajendran, Synthesis and electrochemical characterization of porous niobium oxide coated 316L SS for orthopedic applications, Materials Chemistry and Physics 119 (2010) 363–366.
[9] C.E. Schmidt, V.R. Shastri, J.P. Vacanti, R. Langer, Stimulation of neurite outgrowth using an electrically conducting polymer, Proceedings of the National Academy of Sciences of the United States of America 94 (1997) 8948–8953.
[10] N. Alikacem, Y. Marois, Z. Zhang, B. Jakubiec, R. Roy, M.W. King, R. Guidoin, Tissue reactions to polypyrrole-coated polyesters: a magnetic resonance relaxometry study, Artificial Organs 23 (1999) 910–919.
[11] Wahid Khan, Mamta Kapoor, Neeraj Kumar, Covalent attachment of proteins to functionalized polypyrrole-coated metallic surfaces for improved biocompatibility, Acta Biomaterialia 3 (2007) 541–549.
[12] B. Garner, A. Georgevich, A.J. Hodgson, L. Liu, G.G. Wallace, Polypyrrole–Heparin composites as stimulus-responsive substrate for endothelial cell growth, Journal of Biomedical Materials Research 44 (1999) 121–129.
[13] E. De Giglio, M.R. Guascito, L. Sabbatini, G. Zambonin, Electropolymerization of pyrrole on titanium substrates for the future development of new biocompatible surfaces, Bio Materials 22 (2001) 609–2619.
[14] X. Cui, J. Wiler, M. Dzaman, R.A. Alttchuler, D.C. Martin, In vivo studies of polypyrrole/peptide coated neural probes, Bio Materials 24 (2003) 777–7787.
[15] K. Kawai, N. Mihara, S. Kuwabata, H. Yoneyama, Electrochemical synthesis of polypyrrole films containing TiO_2 powder particles, Journal of the Electrochemical Society 137 (1990) 1793–1796.
[16] F. Beck, M. Dahlhaus, N. Zahedi, Anodic codeposition of polypyrrole and dispersed TiO_2, Electrochimica Acta 37 (1992) 1265–1272.
[17] C.A. Ferreira, S.C. Domenech, P.C. Lacaze, Synthesis and characterization of polypyrrole/TiO_2 composites on mild steel, Journal of Applied Electrochemistry 31 (2001) 49–56.
[18] M. Karthega, S. Nagarajan, N. Rajendran, In vitro studies of hydrogen peroxide treated titanium for biomedical applications, Electrochimica Acta 55 (2010) 2201–2209.
[19] V. Raman, S. Tamilselvi, N. Rajendran, Electrochemical impedance spectroscopic characterization of titanium during alkali treatment and apatite growth in simulated body fluid, Electrochimica Acta 52 (2007) 7418–7424.
[20] M. Karthega, V. Raman, N. Rajendran, Influence of potential on the electrochemical behavior of b titanium alloys in Hank's solution, Acta Biomaterialia 3 (2007) 1019–1023.

[21] T. Kokubo, H. Takadama, How useful is SBF in predicting in vivo bone bioactivity, Biomaterials 27 (2006) 2907–2915.
[22] P. Ocon, A.B. Cristobal, P. Herrasti, T. Fatas, Corrosion performance of conducting polymer coatings applied on mild steel, Corrosion Science 47 (2005) 649–662.
[23] X. He, G. Shi, Electrochemical actuator based on monolithic polypyrrole–TiO_2 nanoparticle composite film, Sensors and Actuators B115 (2006) 488–493.
[24] R. Kostic, D. Rakovic, S.A. Stepanyan, I.E. Davidova, L.A. Gribov, Vibrational spectroscopy of polypyrrole theoretical study, The Journal of Chemical Physics 102 (1995) 3104–3109.
[25] Mingkai Shengying Li, Lijun Chen, Fei He, Xu, Guohu Zhao, Preparation and characterization of polypyrrole/TiO_2 nanocomposite and its photocatalytic activity under visible light irradiation, Journal of Materials Research 24 (2009) 2547–2554.
[26] W.X. Zhang, X.G. Wen, S. Yang, Synthesis and characterization of uniform arrays of copper sulfide nanorods coated with nanolayers of polypyrrole, Langmuir 19 (2003) 4420–4426.
[27] T. Lindgren, J.H. Meabora, E. Avendeno, J. Jonsson, A. Hoel, C.G. Granquist, S.E. Lindquis, Photoelectrochemical and optical properties of nitrogen doped titanium dioxide films prepared by reactive DC magnetron sputtering, The Journal of Physical Chemistry B107 (2003) 5709–5716.
[28] M. Bazzaoui, L. Martins, E.A. Bazzaoui, J.I. Martins, New single-step electrosynthesis process of homogeneous and strongly adherent polypyrrole films on iron electrodes in aqueous medium, Electrochimica Acta 47 (2002) 2953–2962.
[29] Haldorai Yuvaraj, Eun Ju Park, Yeong-Soon Gal, Kwon Taek Lim, Synthesis and characterization of polypyrrole–TiO_2 nanocomposites in supercritical CO_2, Colloids and Surfaces A: Physicochemical and Engineering Aspects 313 (2008) 300–303.
[30] A. Fossati, F. Borgioli, E. Galvanetto, T. Bacci, Corrosion resistance properties of glow-discharge nitrided AISI 316L austenitic stainless steel in NaCl solutions, Corrosion Science 48 (2006) 513–527.
[31] Chih-Neng Chang, Fan-Shiong Chen, Wear resistance evaluation of plasma nitrocarburized AISI 316L stainless steel, Materials Chemistry and Physics 82 (2003) 281–287.
[32] P. Herrasti, L. Díaz, P. Ocón, A. Ibáñez, E. Fatas, Electrochemical and mechanical properties of polypyrrole coatings on steel, Electrochimica Acta 49 (2004) 3693–3699.
[33] P. Herrasti, A.N. Kulak, D.V. Bavykin, C. Ponce de Leonb, J. Zekonytec, F.C. Walsh, Electrodeposition of polypyrrole–titanate nanotube composites coatings and their corrosion resistance, Electrochimica Acta 56 (2011) 323–328.
[34] G. Pujar, N. Parvathavarthini, R.K. Dayal, Some aspects of corrosion and film formation of austenitic stainless steel type 316LN using electrochemical impedance spectroscopy (EIS), Journal of Materials Science 42 (2007) 4535–4544.
[35] Srinivasan Nagarajan, Marimuthu Mohana, Pitchaimuthu Sudhagar, Vedarajan Raman, Toshiyasu Nishimura, Sanghyo Kim, Yong Soo Kang, Nallaiyan Rajendran, Nanocomposite coatings on biomedical grade stainless steel for improved corrosion resistance and biocompatibility, ACS Applied Materials & Interfaces (2012)http://dx.doi.org/10.1021/am301559r.
[36] A. Balamurugan, G. Balossier, S. Kannan, J. Michel, J. Faure, S. Rajeswari, Electrochemical and structural characterisation of zirconia reinforced hydroxyapatite bioceramic sol–gel coatings on surgical grade 316L SS for biomedical applications, Ceramics International 33 (2007) 605–614.
[37] Yong Huang, Yajing Yan, Xiaofeng Pang, Electrolytic deposition of fluorine-doped hydroxyapatite/ZrO_2 films on titanium for biomedical applications, Ceramics International 39 (2013) 245–253.
[38] Rameshbabu Nagumothu Venkateswarlu Kotharu, Chandra Bose Arumugam, Muthupandi Veerappan, Subramanian Sankaran, MubarakAli Davoodbasha, Thajuddin Nooruddin, Fabrication of corrosion resistant, bioactive and antibacterial silver substituted hydroxyapatite/titania composite coating on Cp Ti, Ceramics International 38 (2012) 731–740.
[39] M. Karthega, N. Rajendran, Hydrogen peroxide treatment on Ti–6Al–4V alloy: a promising surface modification technique for orthopedic application, Applied Surface Science 256 (2010) 2176–2183.
[40] K. Bavya Devi, Kulwant Singh, N. Rajendran, Sol–gel synthesis and characterisation of nanoporous zirconium titanate coated on 316L SS for biomedical applications, Journal of Sol–Gel Science and Technology 59 (2011) 513–520.
[41] R. Paital, B. Dahotre, Calcium phosphate coatings for bioimplant applications: materials, performance factors, and methodologies, Materials Science and Engineering: R 66 (2009) 1–70.
[42] K. Bavya Devi, Kulwant Singh, N. Rajendran, Synthesis and characterization of nanoporous sodium-substituted hydrophilic titania ceramics coated on 316L SS for biomedical applications, Journal of Coatings Technology 8 (2011) 595–604.
[43] Jiaguo Yu, Xiujian Zhao, Qingnan Zhao, Gao Wang, Preparation and characterization of super-hydrophilic porous TiO_2 coating films, Materials Chemistry and Physics 68 (2001) 253–259.
[44] H. Zreiqat, M. Valenzuela, Besim Ben Nissan, Richard Roest, Christine Knabe, J. Radlanski, Herbert Renz, J. Evans, The effect of surface chemistry modification of titanium alloy on signalling pathways in human osteoblasts, Bio Materials 26 (2005) 7579–7586.
[45] N. Hijon, M.R. Cabanas, I. Izquierdo barba, M. Vallet regi, Bioactive carbonate–hydroxyapatite coatings deposited onto Ti6Al4V substrate, Chemistry of Materials 16 (2004) 1451–1455.
[46] H.A. El Batal, E.M.A. Khalil, Y.M. Hamdy, In vitro behavior of bioactive phosphate glass–ceramics from the system P_2O_5–Na_2O–CaO containing titania, Ceramics International 35 (2009) 1195–1204.
[47] M. Aziz Kerrzo, K.G. Conrog, A.M. Fenelon, S.T. Farrell, C.B. Breslin, Electrochemical studies on the stability and corrosion resistance of titanium-based implant materials, Bio Materials 22 (2001) 1531–1539.
[48] Wojciech Chrzanowski Ensanya Ali Abou Neel, David Andrew Armitage, Jonathan Campbell Knowles, Effect of surface treatment on the bioactivity of nickel–titanium, Acta Biomaterialia 4 (2008) 1969–1984.
[49] K. Indira, U. Kamachi Mudali, N. Rajendran, Corrosion behavior of electrochemically assembled nanoporous titania for biomedical applications, Ceramics International. http://dx.doi.org/10.1016/j.ceramint.2012.07.013.